JOURNAL OF AIRCRAFT
Vol. 44, No. 2, March–April 2007

Adaptive Compensation Control of Synthetic Jet Actuator Arrays for Airfoil Virtual Shaping

Dipankar Deb* and Gang Tao†
University of Virginia, Charlottesville, Virginia 22903
Jason O. Burkholder‡
Barron Associates, Inc., Charlottesville, Virginia 22901
and
Douglas R. Smith§
University of Wyoming, Laramie, Wyoming 82071

DOI: 10.2514/1.24910

In this paper, a new technology for control of next generation airplanes with virtual aerodynamic wing shaping using synthetic jet actuators is presented. The synthetic jets modify the local flow using a voltage driven vibrating diaphragm. The actuator array outputs are controlled by modulating the peak-to-peak amplitude of the input voltage. Nonlinear parameterized models of synthetic jet actuators whose parameters are chosen from a baseline model are presented. Adaptive inverse arrays are employed for canceling the effect of the jet nonlinearities. A state feedback control law is used for controlling aircraft dynamics. Parameter projection-based adaptive laws are used to ensure desired closed-loop stability and asymptotic tracking. An adaptive inverse scheme that is robust to modeling errors and parametric uncertainties of the synthetic jets is also presented.

Nomenclature

$A \in R^{n\times n}$, $B \in R^{n\times n}$	=	aircraft dynamics matrices
$A_{ppi} = v_i$	=	peak-to-peak voltage applied to the synthetic jet arrays
$C_{\mu ij}$	=	momentum coefficient of the jets (ratio of the jet momentum flux to the freestream momentum flux)
$d_i(t) \in R$	=	known functional components of disturbances
$e(t)$	=	$x(t) - x_m(t)$: tracking errors
$f_{li}(t)$	=	parameter projection functions
i	=	$1, \ldots, 6$, index of synthetic jet arrays
j	=	$1, \ldots, n_i$, index of synthetic jet actuators in ith array
K_1	=	$[K_{11}^T, \ldots, K_{16}^T]^T$: feedback control gain matrix
k_2	=	$[k_{21}, \ldots, k_{26}]^T$: feedforward control vector
$k_{3i}(t)$	=	adaptive estimates of k_{3i}^* for the ith jet array
$k_{3i}^* \in R$	=	unknown amplitudes of disturbances acting on the ith array
l	=	1, 2, index of parameters of synthetic jet actuators
n_i	=	number of synthetic jet actuators in the ith array
$P, Q \in R^{n\times n}$	=	positive definite matrices in Lyapunov equation
p_{1ij}	=	maximum deflection produced by synthetic jet actuators
p_{kij} $(k = 2, 3, 4)$	=	physical parameters of the jets
Q_1, R	=	weighting matrices of the algebraic Riccati equation
$r(t)$	=	bounded reference signal
U_∞	=	free airstream velocity on airfoil
u_d	=	desired state feedback control signals
$x = [x_1, x_2, x_3]^T$	=	aircraft states: roll rate, pitch rate, and yaw rate
$x_m = [x_{m1}, x_{2m}, x_{3m}]^T$	=	reference states: roll rate, pitch rate, and yaw rate
x_m^∞	=	desired final values of reference states
$\gamma_{1i}, \gamma_{2i}, \gamma_{3i}$	=	adaptation gains
η_i	=	gain uncertainties on each array of jets
$\theta_{1i}(t), \theta_{2i}(t)$	=	adaptive estimates of $\theta_{1i}^*, \theta_{2i}^*$ for the ith jet array
$\tilde{\theta}_{1i}, \tilde{\theta}_{2i}$	=	synthetic jet array parameter errors
$\theta_{li}(0)$	=	initial estimates of θ_{li}^*
θ_{li}^a	=	lower bounds of true nonlinearity parameters θ_{li}^*
θ_1^*, θ_2^*	=	true nonlinearity parameters

Received 1 May 2006; revision received 10 July 2006; accepted for publication 10 July 2006.

*Graduate Student, Department of Electrical and Computer Engineering. Student Member AIAA.
†Associate Professor, Department of Electrical and Computer Engineering.
‡Senior Research Scientist, 1410 Sachem Place, Suite 202. Member AIAA.
§Associate Professor, Department of Mechanical Engineering. Senior Member AIAA.

I. Introduction

As new and more sophisticated devices are employed in aircraft control systems to meet new and more demanding flight objectives, the uncertainties associated with these devices become increasingly important in the development of control strategies for a desired system performance. One area that has seen an increased interest recently is in the use of active flow control devices, such as synthetic jet actuators to modify, in a desirable way, the aircraft aerodynamic performance.

The usage of synthetic jet actuators, which have inherent nonlinearities, requires the development of an effective control methodology. One such technique is adaptive inverse compensation which cancels actuator nonlinearities so that full authority control is achieved.

A. Aerodynamic Flow Control on Airplanes

Historically, the premise for good aircraft design has been good aerodynamic performance throughout the aircraft flight envelope. This premise has changed in recent times, particularly for military aircraft, as unconventional aircraft mission objectives increasingly drive the aircraft design. To some degree, many modern military aircraft exhibit shape characteristics that are optimized for nonaerodynamic performance such as low radar cross section. In the future, one can envision aircraft where the design is driven even more by a need to optimize one or more nonaerodynamic performance criteria. For example, future generation aircraft may have wing shapes, where the aerodynamic performance is significantly compromised leading to susceptibility to flow separation and stall at moderate angles of attack (early stall). In such a situation, the wing may require active or passive flow control to achieve acceptable aerodynamic performance.

Passive control devices, such as vortex generators, have been used to improve the aerodynamic performance of wings under certain conditions; however, they afford no proportional control and typically incur an undesirable drag penalty. To obtain a variable control effect, one must use an active flow control approach where the control effect can be modulated as the need for control changes.

An active flow control approach using synthetic jet actuators is particularly attractive because these actuators synthesize a jet from the fluid in which they are immersed without the need for an external source of fluid; hence, they are zero net mass flux in nature. Most importantly, flow control studies have shown that synthetic jet actuators are efficient devices for controlling separated flows [1,2] and for creating virtual surface shape changes.

1. *Flow Separation Control*

Synthetic jet actuators have been used to modify the fluid flow over unconventional airfoils to achieve desired aerodynamic performance [3]. Amitay et al. [4] and Crook and Wood [5] investigated the use of synthetic jet actuators on a symmetric airfoil under different wind tunnel testing conditions. In these studies, the synthetic jet control was used to prevent boundary layer separation at high angles of attack, realizing large gains in lift and dramatic reductions in drag. In addition, the airfoil surface pressure distributions were studied at different angles of attack and for different positions (i.e., azimuthal angles) of actuation around the airfoil nose. These results gave an improved understanding of the effect of reattached flow on the strength of the control inputs.

Recent related flow control work by Washburn and Amitay [6] on a low-speed UAV configuration demonstrated that synthetic jets can not only to control separation on the wing at high angles of attack, but can also be used for roll and pitch control of the vehicle. The authors also showed how the modulation frequency of the synthetic jet actuator could be used as a control variable in manipulating the vehicle attitude.

2. *Virtual Shaping of Airfoils*

The second possible application of synthetic jets is in virtual shaping of an airfoil. The effect was first demonstrated on a circular cylinder model by Honohan et al. [7], who showed that in the mean, synthetic jet actuators can displace flow streamlines and create apparent closed flow regions adjacent to a surface and downstream of the actuator.

In an effort to create a similar effect on an airfoil, Chatlynne et al. [8] used a synthetic jet actuator in conjunction with a small surface obstacle that caused flow separation. By placing a synthetic jet actuator downstream of the obstruction, a stationary recirculating flow domain was established. The effect is a virtual shape change in the airfoil (see Fig. 1).

The top sketch shows the streamlines around a clean airfoil without separation and flow control. The bottom sketch illustrates how synthetic jet flow control might be used to reattach a separated flow to create airfoil virtual shape change. The separation bubble has an attendant pressure distribution that differs from the pressure distribution on the clean airfoil. The height of this bubble is

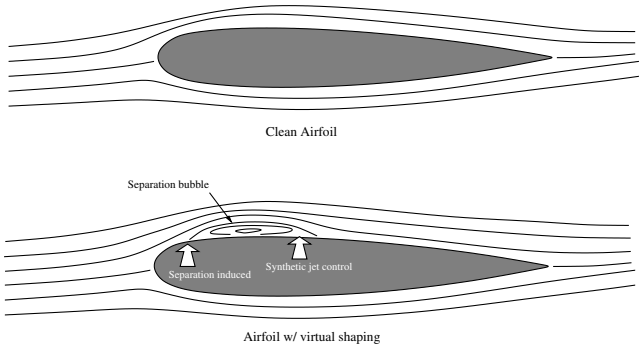

Fig. 1 Illustration of the change in flow streamlines from virtual shaping.

exaggerated for clarity. The synthetic jet controlled the degree to which the flow was separated and consequently the extent to which the apparent shape of the airfoil surface was changed. The obstruction resulted in increased suction in the vicinity of the actuator and pressure reduction in the recovery domain. This work suggests that the lift and pressure distributions might be modified dynamically to achieve a particular flight control objective.

Chen and Beeler [9] designed a two-dimensional NACA 0015 airfoil model to test the mild maneuvering capability of synthetic jets in a subsonic wind tunnel environment. Synthetic jet actuation under different operating conditions was investigated, and the effect of virtual shape change was indicated by a localized increase of surface pressure in the vicinity of jet actuation at low angles of attack.

Finally, one can conceive of a deployment of synthetic jet actuators over an airplane wing surface leading to a reduction, or even an elimination, of mechanical control surfaces on the airplane with an attendant reduction in vehicle cost and weight, and reduction in mechanical complexity. From this brief review of recent work, three means can be identified by which synthetic jets can potentially be used for aerodynamic and flight control.

1) Synthetic jets can be used for separation control at high angles of attack, increasing aircraft maneuverability;

2) when used in conjunction with a separation-inducing device (e.g., boundary layer trip) at low angles of attack, synthetic jets can deflect the flow streamlines creating a new virtual shape of the airfoil so as to reduce drag and/or to increase lift under normal flight conditions; and

3) by distributing individually addressable arrays of synthetic jets over the lifting surface, proportional separation control at high angles of attack can be achieved for aircraft control.

B. Adaptive Inverse Control Technique

Wind tunnel investigations have found that the input signals needed to achieve active flow control objectives using synthetic jet actuator arrays exhibit a highly complex nonlinear relationship between the flight regime and the input signal amplitude, waveform, and frequency [2]. Because of the impracticality of attaining comprehensive, wind tunnel-validated models, describing the effect of synthetic jet arrays over the wide range of potential operating conditions, the use of an adaptive technique should be investigated. Such an approach would allow robust, closed-loop aircraft control using synthetic jet arrays. This *adaptive inverse* methodology [10,11] overcomes prior limitations and sets the stage for practical flight control using synthetic jet actuators to achieve virtual aerodynamic shaping.

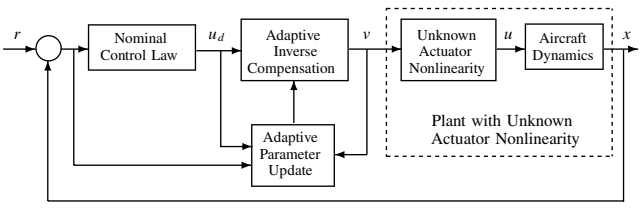

Fig. 2 Adaptive inverse technique block diagram.

The key features of the adaptive inverse approach are shown below in Fig. 2. The essence of this approach is that, upon an adaptation transient, the compensator cancels the effects of the unknown nonlinear actuator characteristic so that a significant improvement in accuracy and performance is achieved. In other words, the controller adaptation is able to remove the unknown component nonlinearity so that a desired system behavior is realized. Note that the adaptive inverse compensator is integrated with the existing nominal flight control system for the aircraft.

In this paper, we focus on developing this adaptive compensation scheme for the second of the three possible synthetic jet applications listed at the end of Sec. I.A. The adaptive control scheme is required to make active flow control viable for virtual surface shaping, by canceling the effect of unknown jet nonlinearities, and updating inverse parameters from projection-based adaptive laws.

The paper is organized as follows. In Sec. II, we provide a physical distribution and mathematical model of the arrays of synthetic jet actuators. In Sec. III, we propose and analyze arrays of adaptive inverse compensation models to cancel the effect of the unknown actuator nonlinearities. We also present some inverse related issues and analyze the control error caused by the parametric uncertainties. In Sec. IV, we present a state feedback control law. In Sec. V we design parameter projection-based adaptive laws, and in Sec. VI we provide stability analysis with such adaptive laws. In Sec. , we present simulation results to illustrate the effectiveness of the adaptive inverse compensation scheme.

II. Synthetic Jet Arrays for Aircraft Flight Control

In this section, we first give a physical description of a synthetic jet actuator and explain how it alters the virtual shape of an airfoil. We then present a mathematical model of the actuator nonlinearity. We also present a possible distribution of synthetic jet arrays on an airfoil and a mathematical model of the parameterized actuator array nonlinearities.

A. Physical Description

A synthetic jet actuator is a zero-net mass flux device that produces a nonzero fluid momentum flux across an orifice. To accomplish this effect, an oscillating pressure gradient is imposed across the orifice by the motion of a piezoelectrically driven diaphragm in a cavity connected to the orifice. As a result of the oscillating pressure gradient, fluid is alternately ingested and expelled through the orifice. As the fluid is expelled, a vortex ring forms and by self-induction, the ring moves away from the orifice. A periodic repetition of this process leads to the formation of a train of vortices that ultimately break down and form a steady, turbulent jet, or synthetic jet as shown in Fig. 3.

Synthetic jet actuators can be constructed in a variety of ways, but the work described herein employs a resonant cavity device (i.e., Helmholz resonator) where the cavity is driven by a piezoelectrically actuated metal diaphragm. The appealing characteristics of this type of synthetic jet actuator is that the piezoelectric diaphragm is primarily a capacitive electrical load that is driven at, or near, its resonant frequency. The actuator cavity is designed to match this frequency; consequently, the power consumption of these devices at peak output is quite low. Synthetic jet actuators of this type are compact and require only a sinusoidal voltage input. The ensuing synthetic jet tends also to be small, issuing from an actuator orifice that is a high-aspect-ratio rectangle (aspect ratio = 100) with minimum dimension as small as 0.5 mm.

We propose an innovative arrangement which expands on the experiments documented by Chatlynne et al. [8]. This arrangement is characterized by synthetic jet actuators located on the airfoil downstream of boundary layer obstacles that cause local flow separation. The synthetic jets control the streamwise extent of the separation region, and the attendant change in the surface pressure distribution gives force and moment increments that can be used for flight control. The proposed arrangement represents a potential means for the future replacement of conventional hydraulically controlled surfaces with synthetic control surfaces.

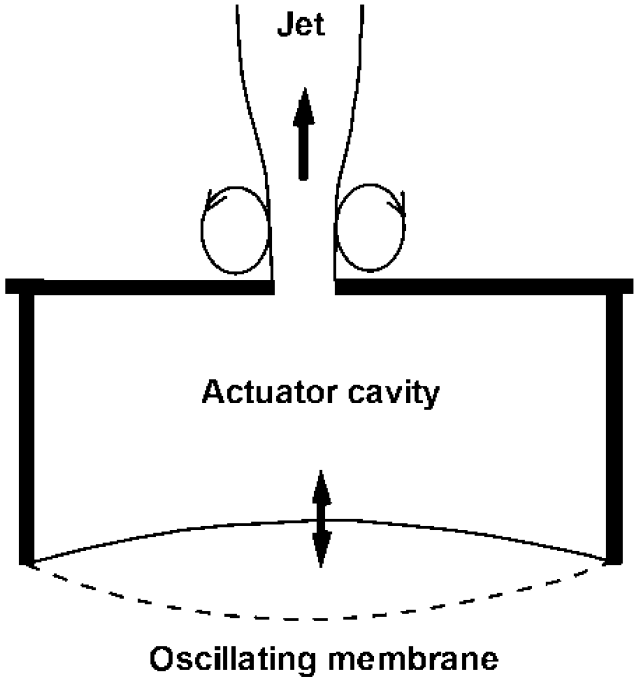

Fig. 3 Synthetic jet actuator [12].

B. Mathematical Model of Jet Arrays

Consider six arrays of synthetic jet actuators. An example of these arrays will be presented in Sec. VII. Each synthetic jet can be characterized by a nonlinearity $N_{ij}(\cdot)$:

$$u_{ij}(t) = N_{ij}[v_i(t)] \tag{1}$$

where $v_i(t) = A^2_{\text{ppi}}(t)$ is the peak-to-peak voltage acting on each array of jets, and $u_{ij}(t)$ is the airfoil virtual surface deflection (output of the actuators) due to each synthetic jet. This virtual airfoil deflection produces an effect similar to the forces and moments generated by the mechanical surfaces. For our adaptive nonlinearity compensation, we also make the realistic assumptions that 1) the output $u_{ij}(t)$ of $N_{ij}(\cdot)$ is not accessible for measurement, and 2) the lower bounds of the parameters of $N_{ij}(\cdot)$ are known from physical dimensions of jets.

For a given actuator design, the actuator resonant frequency f_{act} is constant. The actuator output decreases in nonlinear fashion as the operating frequency moves away from the resonance frequency. In theory, one could control the actuator output through this frequency, but it is simpler and more efficient to do it through the peak-to-peak voltage amplitude. Typically, the actuator output, measured in terms of an averaged orifice velocity, increases with input voltage up to a saturation point. To gain some control of the flow in the frequency domain, the actuator frequency could be modulated at a frequency f_{mod} that is lower than the resonance frequency.

C. Nonlinearity Models

The parametric model for a synthetic jet actuator has been developed ([13,14]). The synthetic jets are actuated so that the control signal generated changes the virtual shape of the airfoil. The jet momentum is assumed to be constant during the entire period of the diaphragm motion. Under conditions of constant airstream density and flow characteristics along the spanwise length of the orifice, the airfoil surface deflection due to the synthetic jet actuators, can be modeled as

$$u_{ij}(t) = p_{1ij} - \frac{p_{2ij}p_{3ij}U_{\infty ij}}{fcC_{\mu ij}(t)}, \qquad i = 1,\ldots,6, \qquad j = 1,\ldots,n_i \tag{2}$$

where $C_{\mu ij} = p_{4ij}A^2_{\text{ppi}}/U^2_{\infty ij}$, c is the local aerodynamic chord, f is the frequency, the parameters p_{kij}, $k = 1,\ldots,4$, $i = 1,\ldots,6$, and

$j = 1, \ldots, n_i$ are assumed to be positive scalar values. These are unknown physical parameters for which the adaptive control scheme compensates. The general form of the model is obtained from a baseline model based on the virtual shaping effect on a real 2-D wing.

The control effect expressed in Eq. (2) was not derived from first principles, rather it is an empirical result obtained from experimental data. We control the actuator output by controlling the peak-to-peak voltage amplitude. To perform adaptive compensation, a parametric model is obtained. The parameterized model for the jth synthetic jet actuator in the ith array is given by

$$u_{ij}(t) = \theta^*_{2ij} - \frac{\theta^*_{1ij}}{v_i(t)}, \qquad i = 1, \ldots, 6, \qquad j = 1, \ldots, n_i \tag{3}$$

where $\theta^*_{ij} = [\theta^*_{1ij}, \theta^*_{2ij}]^T$, $\theta^*_{2ij} = p_{1ij}$, and $\theta^*_{1ij} = p_{2ij}p_{3ij}U^3_{\infty ij}/fcp_{4ij}$.

Because only one input signal $v_i(t)$ is available for each array, we present an array-based adaptive compensation framework in order to be able to define physically meaningful inverses. Based on the physical parameters of the jets, a reformulation of the jet nonlinearities $N_{ij}(\cdot)$ into jet array nonlinearities $N_i(\cdot)$ can be expressed as

$$u_i(t) = \sum_{j=1}^{n_i} \alpha^*_{ij} u_{ij}(t) = \theta^*_{2i} - \frac{\theta^*_{1i}}{v_i(t)}, \qquad i = 1, 2, \ldots, 6 \tag{4}$$

where α^*_{ij} are constant parameters, $\theta^*_i = [\theta^*_{1i}, \theta^*_{2i}]^T$, $\theta^*_{2i} = \sum_{j=1}^{n_i} \alpha^*_{ij}\theta^*_{2ij}$, and $\theta^*_{1i} = \sum_{j=1}^{n_i} \alpha^*_{ij}\theta^*_{1ij}$.

The lift force generated by a synthetic jet actuator array is given by

$$L_i(t) = \bar{q}Su_i(t), \qquad i = 1, \ldots, 6$$

where $\bar{q}$ is the freestream dynamic pressure, and S the surface area of the wing. These forces are equivalent to lift forces generated by mechanical control surfaces. However, in this paper, we study the adaptive control of synthetic jet actuator arrays whose output (input to aircraft dynamics) is the virtual surface deflection, rather than the equivalent lift force. The key features of the synthetic jet array nonlinearity model as given in Eq. (4) are that the structure of the model is known, and the lower bounds of the parameters θ^*_{1i} and θ^*_{2i} are known. These are the necessary conditions for developing an adaptive inverse model.

D. Control Inputs

In the aircraft dynamics, the control inputs are the effective synthetic jet array surface deflections $u_i(t)$, from the six synthetic jet arrays. The surface deflections on the outer trailing edge, midflap, and spoiler arrays on the left of the longitudinal axis are represented as $u_1(t)$, $u_3(t)$, and $u_5(t)$, and the surface deflections on the outer, midflap, and spoiler arrays on the right of the longitudinal axis, respectively, are represented as $u_2(t)$, $u_4(t)$, and $u_6(t)$. It is assumed that the outputs $u_i(t)$ of the jet array nonlinearities $N_i(\cdot) = [N_{i1}(\cdot), \ldots, N_{in_i}(\cdot)]^T$ are not accessible for measurement, and only the bounds of the parameters of $N_i(\cdot)$ are known. We will demonstrate that our adaptive compensation framework performs closed-loop feedback control without the inputs being available for measurement and the parameters being poorly known.

For a typical synthetic jet actuator, the parameters $p_1 = 15$, $p_2 = 0.05$, $p_3 = 0.05$, and $p_4 = 5$ are chosen arbitrarily as a baseline model. The values $f = 60$ Hz, and $c = 2$ ft and $U_\infty = 200$ ft/s are taken as reasonable. The simplified model with these parameters is

$$u(t) = 15 - \frac{33.33}{A^2_{\text{pp}}(t)}$$

Variations of deflection on the surface of the airfoil, plotted against actuator voltage magnitude at different values of parameter θ^*_1 of a synthetic jet actuator are shown in Fig. 4.

In the next section, we present an adaptive inverse control scheme for synthetic jet array nonlinearities. It is evident from (4) that the variations of deflection on the wing surface against actuator array voltage magnitudes $v_i(t)$ at different values of parameters θ^*_{1i} of synthetic jet arrays would represent similar characteristics to the one shown in Fig. 4, for a typical synthetic jet model as given in Eq. (3).

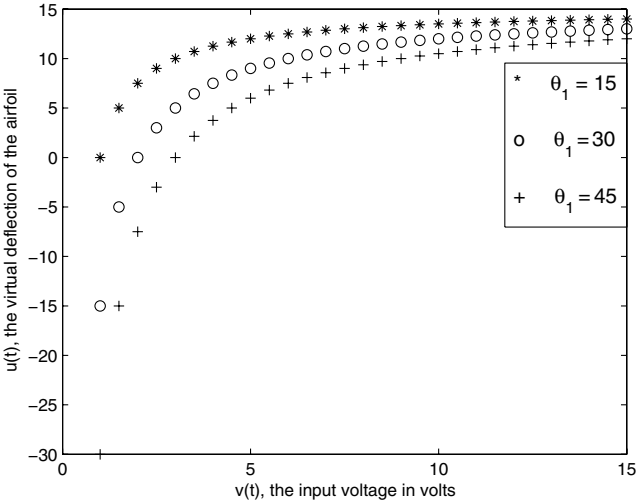

Fig. 4 Variation of virtual surface deflection with actuation voltage.

III. Adaptive Nonlinearity Inverses

The essence of the adaptive inverse compensation approach is to employ an inverse

$$v_i(t) = \widehat{NI}_i[u_{di}(t)] \tag{5}$$

to cancel the effect of the unknown nonlinearity $N_i(\cdot)$, where the inverse characteristic $\widehat{NI}_i(\cdot)$ is parameterized by an estimate $\theta_i(t) = [\theta_{1i}(t), \theta_{2i}(t)]^T$ of θ^*_i, and $u_{di}(t)$ is a desired control signal from a feedback law. The adaptive inverse that compensates for the undesirable effect of jet array nonlinearities in Eq. (4) is given by

$$v_i(t) = \frac{\theta_{1i}(t)}{\theta_{2i}(t) - u_{di}(t)}, \qquad i = 1, \ldots, 6 \tag{6}$$

where $\theta_{1i}(t)$, $\theta_{2i}(t)$ are to be updated from adaptive laws and should remain in prespecified regions, that is,

$$\theta_{1i}(t), \theta_{2i}(t) > 0, \quad \text{because } \theta^*_{1i}, \theta^*_{2i} > 0$$

is needed to implement the inverses. Such adaptive laws are developed based on a parameterized error model, and the parameter boundaries are ensured by parameter projection. For our control problem, we make the assumption:

$$u_{di}(t) < \theta_{2i}(t), \qquad \forall\ t \geq 0, \qquad i = 1, \ldots, 6 \tag{7}$$

where $\theta_{2i}(t)$ represents the maximum surface deflection.

An adaptive compensation framework with the arrays of synthetic jet nonlinearities and the inverse jet arrays are represented as follows in Fig. 5.

The key features of the adaptive inverse approach are the adaptive compensator for the unknown actuator nonlinearity and the feedback adaptation for updating the compensator parameters. The essence of this approach is that, upon an adaptation transient, the compensator cancels the effects of the unknown nonlinear actuator characteristic so that a significant improvement of accuracy and performance is achieved. In other words, the adaptation of the controller is able to remove the unknown component nonlinearity so that a desired behavior of the system is realized.

Note that the adaptive inverse compensator is integrated with the existing nominal guidance and control system for the aircraft. The nominal flight control system can be designed using any adaptive or nonadaptive feedback technique without considering the actuator nonlinearity. The adaptive inverse control technique can be successfully applied to synthetic jet actuators without extensive wind tunnel tests because the synthetic jet model structure is known.

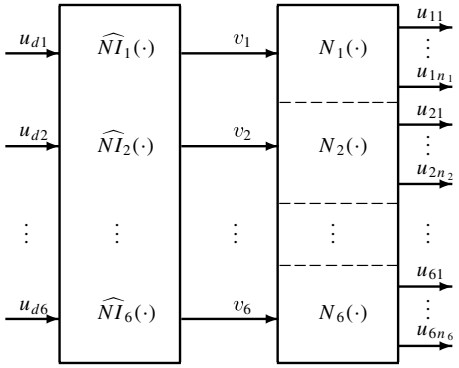

Fig. 5 Adaptive compensation for synthetic jet arrays.

A. System Error

Adaptive control systems use system errors to adjust controller parameters to obtain desired performance. Using Eqs. (4) and (6), we obtain

$$u_i(t) = \frac{\theta^*_{2i}\theta_{1i}(t) - \theta^*_{1i}[\theta_{2i}(t) - u_{di}(t)]}{\theta_{1i}(t)} \tag{8}$$

Thus, the control error is given by

$$u_i(t) - u_{di}(t) = \frac{\theta^*_{2i}\theta_{1i}(t) - \theta^*_{1i}\theta_{2i}(t) + u_{di}(t)\theta^*_{1i} - u_{di}(t)\theta_{1i}(t)}{\theta_{1i}(t)}$$

Rearranging, we obtain

$$u_i(t) - u_{di}(t) = \left(\frac{\theta_{2i}(t) - u_{di}(t)}{\theta_{1i}(t)}\right)\tilde{\theta}_{1i}(t) - \tilde{\theta}_{2i}(t) \tag{9}$$

where $\tilde{\theta}_{1i} = \theta_{1i}(t) - \theta^*_{1i}$, and $\tilde{\theta}_{2i} = \theta_{2i}(t) - \theta^*_{2i}$.

IV. Feedback Control System

In this section, we present a state feedback adaptive inverse control scheme to cancel $N_i[\theta^*_i; v_i(t)]$, $\forall\ i = 1, \ldots, 6$ to meet the control objective. Such a control system is shown in Fig. 6 [note that the output $y(t)$ is not used in this study]. This control system is a special case of the general structure shown in Fig. 2. In this case, the linear state feedback control law is $u_d = -K_1 x + k_2 r$, the adaptive inverse $v(t) = \widehat{NI}[u_d(t)]$ is to be updated from an adaptive law (not shown in Fig. 2), the aircraft dynamics block is $\dot{x} = Ax + Bu$, and the actuator nonlinearity block is $u = N(v)$.

We consider a linearized model of aircraft dynamics with synthetic jet actuators. Such a system that has a controllable state variable form can be described by

$$\dot{x}(t) = Ax(t) + Bu(t) = Ax(t) + \sum_{i=1}^{6}\sum_{j=1}^{n_i} b_{ij}u_{ij}$$

$$= Ax(t) + \sum_{i=1}^{6} b_i u_i, \qquad x \in R^n \tag{10}$$

where $B = [b_1, \ldots, b_6] \in R^{n\times 6}$, provided we assume that $b_{ij} = \xi_{ij}b_{ik}$, $j \neq k$, $j, k \in 1, 2, \ldots, n_i$, where ξ_{ij} are proportionality constants. To stabilize such a system, the desired state feedback control signal is

$$u_d(t) = -K_1^T x(t) + k_2 r(t) \tag{11}$$

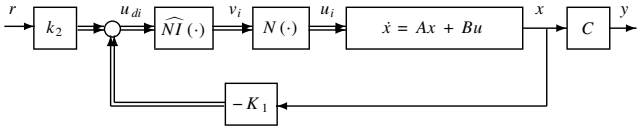

Fig. 6 State feedback inverse control system.

where $u_d(t) = [u_{d1}, \ldots, u_{d6}]^T$, and K_1 is chosen such that $A - BK_1$ are equal to some desired closed-loop poles. The choice of K_1 can be made from a pole placement [15] or a linear quadratic optimal control design [16]. Using Eqs. (6), (10), and (11), the closed-loop linear system dynamics are

$$\dot{x}(t) = Ax(t) + \sum_{i=1}^{6} b_i\left(u_{di}(t) + \frac{\theta_{2i}(t) - u_{di}(t)}{\theta_{1i}(t)}\tilde{\theta}_{1i} - \tilde{\theta}_{2i}\right)$$

$$= (A - BK_1)x(t) + Bk_2 r(t) + \sum_{i=1}^{6} b_i\left(\frac{\theta_{2i}(t) - u_{di}(t)}{\theta_{1i}(t)}\tilde{\theta}_{1i}(t) - \tilde{\theta}_{2i}(t)\right) \tag{12}$$

where $\sum_{i=1}^{6} b_i K_{1i}^T = BK_1$, and $\sum_{i=1}^{6} b_i k_{2i} = Bk_2$. This equation motivates us to choose a reference model

$$\dot{x}_m(t) = (A - BK_1)x_m(t) + Bk_2 r(t) \tag{13}$$

where $x_m(t)$ represents the desired aircraft state trajectory, and the body axis dynamics are stabilized by the stable matrix $A - BK_1$. The physical meaning of $Bk_2 r(t)$ is the desired external body axis motion command.

The control objective now is to choose the matrix K_1, the vector k_2, and the adaptive laws for $\theta_{1i}(t)$, $\theta_{2i}(t)$, such that the structure and dynamics of the aircraft dynamics are modified such that all closed-loop signals are bounded and $\lim_{t\to\infty}[x(t) - x_m(t)] = 0$.

V. Adaptive Laws

Adaptive laws are usually differential equations whose states are the parameter estimates. The laws are designed using stability considerations to minimize the difference between the system states $x(t)$ and the reference states $x_m(t)$ with respect to parameter estimates at each time instant t. Parameter projection is used to guarantee the boundedness of $\theta_{1i}(t)$, $\theta_{2i}(t)$ by lower bounds so that the adaptive inverses are meaningful. We assume that

$$\theta^a_{1i} \leq \theta^*_{1i}, \qquad \theta^a_{2i} \leq \theta^*_{2i}, \qquad i = 1, \ldots, 6$$

for some known constants θ^a_{1i}, $\theta^a_{2i} > 0$ such that

$$\theta_{1i}(t) > \theta^a_{1i}, \qquad \theta_{2i}(t) > \theta^a_{2i}, \qquad i = 1, \ldots, 6$$

the characteristic $N[\theta_i(t); v_i(t)]$ renders a nonlinearity model of the same type as that of $N[\theta^*_i; v_i(t)]$ given in Eq. (4). Initial estimates $\theta_{1i}(0)$ of θ^*_{1i} and $\theta_{2i}(0)$ of θ^*_{2i} are chosen such that $\theta_{1i}(0) \geq \theta^a_{1i}$ and $\theta_{2i}(0) \geq \theta^a_{2i}$, respectively. We choose the adaptive laws for θ_{li} as

$$\dot{\theta}_{li}(t) = g_{li}(t) + f_{li}(t), \qquad l = 1, 2, \qquad i = 1, \ldots, 6, \qquad t \geq 0 \tag{14}$$

where $f_{li}(t)$ are projection functions to be determined, and the functions $g_{li}(t)$ are given by

$$g_{1i}(t) = -\gamma_{1i}e^T(t)Pb_i\left(\frac{\theta_{2i}(t) - u_{di}(t)}{\theta_{1i}}\right), \qquad g_{2i}(t) = \gamma_{2i}e^T(t)Pb_i$$

with some design parameters γ_{1i}, $\gamma_{2i} > 0$, which control adaptation rates, and $P \in R^{n\times n}$, which is a constant matrix such that $P = P^T > 0$ satisfies the Lyapunov equation

$$P(A - BK_1) + (A - BK_1)^T P = -Q \tag{15}$$

For some constant $Q = Q^T > 0$, with any given Q, and such a P can be determined uniquely.

The projection functions $f_{li}(t)$ have to be such that the boundedness of the parameter estimates are guaranteed. This parameter projection design uses the knowledge of the parameter lower bounds to ensure that the parameter estimates $\theta_{li}(t)$ stay in the same region where their true values $\theta^*_{li}(t)$ stay. For adaptive laws of the form given by Eq. (14), $f_{li}(t)$ are given by

$$f_{li}(t) = \begin{cases} 0 & \text{if } \theta_{li}(t) > \theta^a_{li}, \text{ or} \\ & \text{if } \theta_{li}(t) = \theta^a_{li} \quad \text{and} \quad g_{li}(t) \geq 0, \; l = 1, 2, \; i = 1, \ldots, 6 \\ -g_{li}(t) & \text{otherwise} \end{cases} \tag{16}$$

The implementation of the adaptive laws for $\theta_{li}(t)$ are simple:

$$\theta_{li}(t) = -\int_0^t [g_{li}(\tau) + f_{li}(\tau)]\, \mathrm{d}\tau + \theta_{li}(0)$$

It is important to note that the desired adaptation is achieved by a state feedback mechanism, and it is designed to be robust with respect to time-varying system parameters (it is known that the parameters will vary with operating condition in this application). Additionally, the adaptive inverse technique will ensure closed-loop stability and asymptotic tracking performance.

VI. Stability Analysis

In this section, we first analyze the stability of the adaptive compensation scheme for the aircraft dynamic model in absence of disturbances or gain uncertainties as has been assumed so far in this paper. We also discuss robustness issues, introduce additional adaptive laws to make the controller robust, and analyze the system performance in the presence of some modeling errors.

Theorem VI.1: Under assumption (7), the control laws of Eq. (11), updated from the adaptive laws of Eq. (14), the inverses of Eq. (6) and applied to the plant of Eq. (10), guarantee closed-loop signal boundedness and $\lim_{t\to\infty} e(t) = 0$.

Proof: Using Eqs. (12) and (13), the dynamic equation for tracking error $e(t)$ is given by

$$\dot{e}(t) = (A - BK_1)e(t) + \sum_{i=1}^{6} b_i \left(\frac{\theta_{2i}(t) - u_{di}(t)}{\theta_{1i}(t)} \tilde{\theta}_{1i}(t) - \tilde{\theta}_{2i}(t) \right) \tag{17}$$

Consider the positive definite function

$$V = e^T P e + \sum_{j=1}^{2} \sum_{i=1}^{6} \tilde{\theta}^2_{ji} \gamma^{-1}_{ji} \tag{18}$$

as a measure of e, $\tilde{\theta}_{li}$, and $t \geq 0$. Noting that $\dot{\tilde{\theta}}_{li}(t) = \dot{\theta}_{li}(t)$. The time derivative of V is given by

$$\dot{V} = e^T(t) P \dot{e}(t) + \dot{e}^T(t) P e(t) + 2 \sum_{l=1}^{2} \sum_{i=1}^{6} \tilde{\theta}_{li}(t) \gamma^{-1}_{li} \dot{\theta}_{li}(t) \tag{19}$$

Substituting Eqs. (14), (15), and (17), into Eq. (19), we have

$$\dot{V} = -e^T(t) Q e(t) + 2 \sum_{l=1}^{2} \sum_{i=1}^{6} \tilde{\theta}_{li}(t) \gamma^{-1}_{li} f_{li}(t) \tag{20}$$

With $\theta_{li}(0) \geq \theta^a_{li}$, and from the parameter projection algorithm of Eq. (16), it follows that

$$\theta_{li}(t) \geq \theta^a_{li}, \qquad \tilde{\theta}_{li}(t) f_{li}(t) \leq 0, \qquad l = 1, 2, \qquad i = 1, \ldots, 6 \tag{21}$$

With this property, Eq. (20) reduces to the negative semidefinite time derivative

$$\dot{V} = -e^T(t) Q e(t) \leq 0 \tag{22}$$

From which we have $e(t)$ uniformly bounded, and $e(t) \in L^2$. At the same time, it is guaranteed by parameter projection that $\theta_{li}(t)$ are bounded for $t > 0$. From Eq. (17), $\dot{e}(t)$ is bounded. Therefore, the adaptation scheme ensures that all closed-loop signals are bounded and $\lim_{t\to\infty} e(t) = 0$. □

This means, for the current application, the cancellation of unknown synthetic jet actuator nonlinearities by an adaptive inverse compensation scheme is feasible. Based on this result, adaptive inverse controllers can be designed for progressively more complex and realistic aircraft models and actuator configurations. This theorem guarantees only the boundedness of parameter errors. A theoretical proof of the asymptotic convergence of parameter errors would also require satisfaction of persistence of excitation conditions. Without persistence of excitation conditions, the parameter errors will only converge to a linear space of solutions.

A. Robustness Issues

Sastry and Bodson [17] have studied robustness issues related to adaptive control systems. The plant model of Eq. (10) is free of disturbances and unmodeled dynamics. That is, our analysis has implicitly assumed that the atmosphere is calm and fixed which is rarely true because we must contend with atmospheric turbulence and its interaction with the aerodynamics of the airplane. These motions impact the synthetic jet control of the aircraft model. In particular, the effect of boundary layer disturbances due to the boundary layer trips (which are used for separation enhancers) can be reasonably expressed as $k^*_{3i} d_i(t)$, $i = 1, \ldots, 6$, where k_{3i} are the unknown amplitudes of the disturbances and $d_i(t)$ as the known frequency component of the disturbance.

This disturbance frequency can be determined from dimensional analysis using the size of the boundary layer trip and an appropriate flow velocity. The disturbance frequency scales with the height of the boundary layer trip, h, and the freestream velocity, U_∞, and may be reasonably well approximated as $0.07 \frac{U_\infty}{h}$ [18]. In the event that the frequency of disturbance is not known or due to unsteadiness of the flow, it can be estimated and the estimate can be used in another adaptive compensation algorithm to adjust the magnitude and phase of the input needed to cancel the effect of the disturbance. Such algorithms have been studied by Bodson and Douglas [19], but disturbance rejection with unknown frequency is still very much an open problem.

The adaptive control approach can be employed to reject the effect of bounded disturbances, acting at the vicinity of each synthetic jet array, so that the desired system performance can be achieved using certain additional compensation introduced in the controller. To enhance robustness of our adaptive control scheme in the presence of bounded disturbances, additional adaptive laws are to be designed to ensure closed-loop stability and asymptotic tracking.

All practical forms of gain uncertainties, unmodeled dynamics, and actuation disturbances in synthetic jet arrays that affect the current application are not known at this stage. We do know that there may be transient effects that occur when the actuators are turned on and off or the power level is changed and leading to gain uncertainties. We will demonstrate that our adaptation scheme is robust to this class of gain uncertainties and bounded disturbances described above. In Fig. 7, we represent the synthetic jet actuators acting on an aircraft model in the presence of these gain uncertainties and disturbances.

The adaptive inverse design developed in this paper is already robust to $\eta_i, i = 1, \ldots, 6$. This is because the structure of the model of Eq. (4) does not change due to such gain uncertainties, with only the parameters of the jet array characteristics being modified. Therefore, there is no essential difference in the inverse model employed and the adaptation structure already employed is sufficient.

We consider aircraft dynamics with modeling errors described by

$$\dot{x}(t) = Ax(t) + \sum_{i=1}^{6} b_i u_i(t) + \sum_{i=1}^{6} b_i k^*_{3i} d_i(t), \qquad x \in R^n \tag{23}$$

where $[b_1, \ldots, b_6] = B$. The desired state feedback control signal is modified as

$$u_d(t) = -K_1^T x(t) + k_2 r(t) - k_3(t)d(t) \tag{24}$$

where $r(t)$ is bounded, and $k_3(t)d(t) = [k_{31}(t)d_1(t), \ldots, k_{36}(t)d_6(t)]^T$ are bounded.

Using Eqs. (9) and (23), the closed-loop linear system dynamics are

$$\begin{aligned}\dot{x}(t) &= Ax(t) + \sum_{i=1}^{6} b_i\left(u_{di}(t) + \frac{\theta_{2i}(t) - u_{di}(t)}{\theta_{1i}(t)}\tilde{\theta}_{1i}(t) - \tilde{\theta}_{2i}(t)\right) \\ &\quad + \sum_{i=1}^{6} b_i k_{3i}^* d_i(t) = (A - BK_1)x(t) + Bk_2 r(t) \\ &\quad + \sum_{i=1}^{6} b_i\left(\frac{\theta_{2i}(t) - u_{di}(t)}{\theta_{1i}(t)}\tilde{\theta}_{1i} - \tilde{\theta}_{2i}\right) - B\tilde{k}_3 d(t)\end{aligned} \tag{25}$$

where $\sum_{i=1}^{6} b_i K_{1i}^T = BK_1$, $\sum_{i=1}^{6} b_i k_{2i} = Bk_2$, $\sum_{i=1}^{6} b_i \tilde{k}_{3i} d_i(t) = Bk_3 d(t)$, and $\tilde{k}_{3i}(t) = k_{3i}(t) - k_{3i}^*$.

For a reference model of Eq. (13), the control objective now is to choose the matrix K_1, the vector k_2, and the adaptive laws for $\theta_{1i}(t)$, $\theta_{2i}(t)$, $k_{3i}(t)$, such that closed-loop signals are bounded and $\lim_{t\to\infty}[x(t) - x_m(t)] = 0$.

In addition to the adaptive laws given by Eq. (14), we choose an adaptive law for $k_{3i}(t)$ as

$$\dot{k}_{3i}(t) = \gamma_{3i} e^T(t) P b_i d_i(t), \qquad i = 1, \ldots, 6 \tag{26}$$

where $\gamma_{3i} > 0$ and $P = P^T > 0$ satisfies (15).

Theorem VI.2: Under assumption (7), the control laws of Eq. (11), updated from the adaptive laws of Eqs. (14) and (26), the inverses of Eq. (6) applied to the plant of Eq. (23) guarantee closed-loop boundedness and $\lim_{t\to\infty} e(t) = 0$, in presence of gain uncertainties and bounded disturbances as shown in Fig. 7.

Proof: Using Eqs. (13) and (25), the dynamic equation for tracking error $e(t)$ is given by

$$\begin{aligned}\dot{e}(t) &= (A - BK_1)e(t) + \sum_{i=1}^{6} b_i\left(\frac{\theta_{2i}(t) - u_{di}(t)}{\theta_{1i}(t)}\tilde{\theta}_{1i} - \tilde{\theta}_{2i}\right) \\ &\quad - B\tilde{k}_3 d(t)\end{aligned} \tag{27}$$

Consider the positive definite function

$$V = e^T P e + \sum_{j=1}^{2}\sum_{i=1}^{6} \tilde{\theta}_{ji}^2 \gamma_{ji}^{-1} + \sum_{i=1}^{6} \tilde{k}_{3i}^2 \gamma_{3i}^{-1} \tag{28}$$

as a measure of system errors e and $\tilde{\theta}_{li}$. Noting that $\dot{\tilde{\theta}}_{li}(t) = \dot{\theta}_{li}(t)$, $\dot{\tilde{k}}_{3i}(t) = \dot{k}_{3i}(t)$, $l = 1, 2$, and $i = 1, \ldots, 6$. The time derivative of V is given by

$$\begin{aligned}\dot{V} &= e^T(t)P\dot{e}(t) + \dot{e}^T(t)Pe(t) + 2\sum_{l=1}^{2}\sum_{i=1}^{6} \tilde{\theta}_{li}(t)\gamma_{li}^{-1}\dot{\theta}_{li}(t) \\ &\quad + 2\sum_{i=1}^{6} \tilde{k}_{3i}(t)\gamma_{3i}^{-1}\dot{k}_{3i}(t)\end{aligned} \tag{29}$$

Substituting Eqs. (15), (26), and (27), into Eq. (29), we have

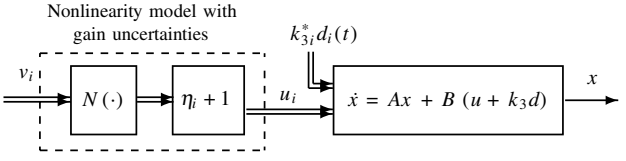

Fig. 7 Aircraft model with jet nonlinearities in presence of gain uncertainties and disturbances.

$$\begin{aligned}\dot{V} &= -e^T(t)Qe(t) + 2e^T(t)P\sum_{i=1}^{6} b_i\left(\frac{\theta_{2i}(t) - u_{di}(t)}{\theta_{1i}(t)}\tilde{\theta}_{1i} - \tilde{\theta}_{2i}\right) \\ &\quad + 2\sum_{l=1}^{2}\sum_{i=1}^{6} \tilde{\theta}_{li}(t)\gamma_{li}^{-1}\dot{\theta}_{li}(t)\end{aligned} \tag{30}$$

Therefore, substituting Eq. (14) into Eq. (30), we get Eq. (20) and by repeating the remaining steps in Theorem VI.1, and noting that $k_{3i}(t)$ are bounded, from Eq. (27) we get that $\dot{e}(t)$ is bounded. Therefore, the adaptation scheme ensures that all closed-loop signals are bounded and $\lim_{t\to\infty} e(t) = 0$, in the presence of gain uncertainties and bounded disturbances as shown in Fig. 7. □

In Secs. II, III, IV, V, and VI, we demonstrated the effectiveness of an adaptive inverse compensation scheme for synthetic jet actuator arrays. In the next section, we evaluate the system performance by undertaking a simulation study on a 3 DOF (degree of freedom) linearized tailless aircraft model, for adaptive compensation of synthetic jet nonlinearities for asymptotic tracking of roll rate, pitch rate, and yaw rates.

VII. System Performance Evaluation

One of the most likely platforms for the application of synthetic jet actuator technology is the new generation of stealth aircrafts designed for reduced radar cross sections and therefore lacking vertical surfaces. Barron Associates, Inc., has developed a medium-fidelity model of an uninhabited combat air vehicle (UCAV), using only unclassified and nonproprietary information. The Barron Associates nonlinear tailless aircraft model (BANTAM) is a blended-wing-body design based on an Air Force Research Laboratories concept drawing. BANTAM captures the essential nonlinearities and is a target platform for the proposed investigation.

For a system performance evaluation of the BANTAM configuration, the spoilers and trailing edge flaps in the model are replaced by six arrays of synthetic jet actuators (six shaded regions) with boundary layer trips located forward in the airstream, as shown in Fig. 8. The jets are distributed symmetrically on the left and right sides of the longitudinal axis. The location of the jets is critical in generating required localized pressure distribution on the airfoil.

The physical parameters of the BANTAM are summarized in Table 1.

The adaptive inverse control technique is applied to a 3 degree of freedom linearized model with six arrays of synthetic jet actuators distributed over the airfoil. We demonstrate the feasibility of canceling synthetic jet actuator nonlinearities using simulation results. Based on this result, adaptive inverse controllers can be designed for progressively more complex and realistic aircraft models and actuator configurations.

We evaluate the performance of our adaptive compensation scheme using a linear quadratic regulator (LQR) design. The simulation for our adaptive inverse control scheme is performed for a 3-DOF linearized aircraft (BANTAM) model for the roll, pitch, and yaw rates

$$x = \begin{bmatrix} x_1 & x_2 & x_3 \end{bmatrix}^T$$

at the trim condition: Mach number $M = 0.455$, angle of attack $\alpha = 2.7$ deg, and side slip angle $\beta = 0$, with six arrays of jets distributed over the airfoil. The matrices $A \in R^{3\times3}$ and $B \in R^{3\times6}$ are obtained analytically from the dimensional aerodynamic coefficients for the BANTAM with mechanical control surfaces.

Matrix A does not include the body moments of the BANTAM, and so simulating the linear dynamic system Eq. (10) does not produce the same result as the full nonlinear system having mechanical control surfaces. However, matrix B accurately predicts the angular accelerations due to the virtual surface deflections. Matrices A and B are given by

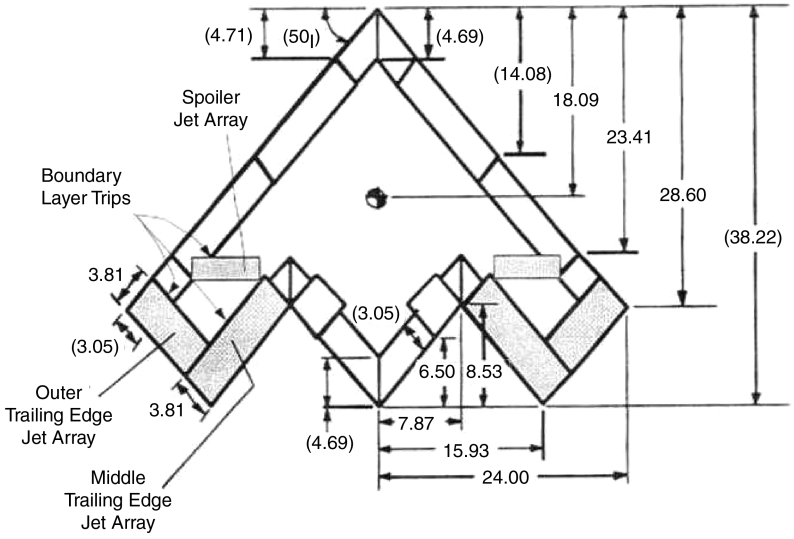

Fig. 8 BANTAM airfoil showing boundary layer trips and six jet arrays (measurements in feet).

$$A = \begin{bmatrix} -61.1273 & 0 & -7.6409 \\ 0 & -174.3472 & 0 \\ -7.2692 & 0 & -0.4543 \end{bmatrix}$$

$$B = \begin{bmatrix} -0.2292 & 0.2292 & -0.2292 & 0.2292 & -0.0306 & 0.0306 \\ 0.0599 & 0.0599 & 0.0804 & 0.0804 & -0.0256 & -0.0256 \\ -0.0084 & 0.0084 & -0.0535 & 0.0535 & 0.1177 & -0.1177 \end{bmatrix}$$

with the inputs $u_i(t)$, $i = 1, 2, \ldots, 6$. The plant has the following open loop poles: -62.0293, 0.4477, and -174.3472. The chosen matrix B indicates the effect that the deflection equivalent to the virtual shaping has on the roll, pitch, and yaw rates.

To have a quantitative understanding of the effect of the virtual deflection caused by the jets in the outer arrays on the aerodynamic motion, let us consider the aircraft dynamics Eq. (10) with the states $x_1(t_0) = 0$, $x_2(t_0) = 0$, and $x_3(t_0) = 0$, where t_0 is the initial time. Consider that only the jets in the outer right array in Fig. 8 are actuated for virtual deflection, that is,

$$u_1(t_0) = 5, \qquad u_2(t_0) = 0, \ldots, u_6(t_0) = 0 \text{ deg} \tag{31}$$

The changes in the roll, pitch, and yaw rates are given by

$$\dot{x}_1(t_0) = -1.146, \qquad \dot{x}_2(t_0) = -0.2955, \qquad \dot{x}_3(t_0) = -0.0420$$

in deg /s^2. If the nose of the BANTAM in Fig. 8 is moving forward parallel to the paper, then the changes in the states cause a counter-counterclockwise roll and downward motion with a counter-clockwise spin. If instead, we consider that

$$u_1(t_0) = 0 \qquad u_2(t_0) = 5, \qquad u_3(t_0) = 0, \ldots, u_6(t_0) = 0 \text{ deg} \tag{32}$$

then from Eq. (10), the changes in the roll, pitch, and yaw rates are given by

$$\dot{x}_1(t_0) = 1.146, \qquad \dot{x}_2(t_0) = -0.2955, \qquad \dot{x}_3(t_0) = 0.0420$$

Table 1 BANTAM physical parameters

Property	Units	Value	Property	Units	Value
Leading edge sweep	deg	50	I_{xx}	slug-ft^2	11,000
Mass	slug	419.3	I_{yy}	slug-ft^2	6,500
Weight	lb	13,500	I_{zz}	slug-ft^2	18,500
Span	ft	32	Aspect ratio	——	2.5
Reference area	ft^2	410	Mean aero. chord	ft	15.3

in deg /s^2. This causes a clockwise roll and downward motion with clockwise spin. These motions with inputs as in Eqs. (31) and (32) are symmetric with respect to the roll axis, which is as expected because the outer right and outer left arrays are physically symmetric with respect to the roll axis.

A similar analysis can be carried out with different actuated arrays to determine the motion of the BANTAM. The desired feedback control law is given by Eq. (11) where $k_2 \in R^{6\times 1}$ is a known vector and $K_1 \in R^{6\times 3}$ is a gain matrix such that for an optimization criterion to place the poles, the quadratic performance index is given by

$$J = \int_{t_0}^{\infty} (x^T Q_1 x + u^T R u)\, \mathrm{d}t$$

with $Q_1 = I_3$ and $R = 0.5 I_6$ is minimized. Using the CARE function in MATLAB, the continuous-time algebraic Riccati equation

$$A^T P_1 + P_1 A - P_1 B R^{-1} B^T P_1 + Q_1 = 0$$

computes the unique stabilizing solution P_1 given by

$$P_1 = \begin{bmatrix} 0.2202 & 0.0000 & -1.7969 \\ 0.0000 & 0.0029 & -0.0000 \\ -1.7969 & -0.0000 & 15.2286 \end{bmatrix}$$

and the gain matrix K_1 as

$$K_1 = R^{-1} B^T P_1 = \begin{bmatrix} -0.0708 & 0.0003 & 0.5679 \\ 0.0708 & 0.0003 & -0.5679 \\ 0.0913 & 0.0005 & -0.8058 \\ -0.0913 & 0.0005 & 0.8058 \\ -0.4365 & -0.0001 & 3.6948 \\ 0.4365 & -0.0001 & -3.6948 \end{bmatrix}$$

With this K_1, we have

$$A - BK_1 = \begin{bmatrix} -61.1446 & 0 & -7.5238 \\ 0 & -174.3473 & 0 \\ -7.1579 & 0 & -1.4007 \end{bmatrix} \tag{33}$$

The closed-loop poles are -62.0328, -0.5125, and -174.3473. The CARE function ensures that the poles of A that are stable are almost the same as those of $A - BK_1$, and only the unstable pole is modified into a stable one. This is the criteria of selection of K_1 for a good adaptive controller. Using $A - BK_1$, $Q = 10 I_3$, and the MATLAB function LYAP, for the Lyapunov matrix equation (15), we obtain

$$P = \begin{bmatrix} 0.2137 & 0 & -1.1270 \\ 0 & 0.0287 & 0 \\ -1.1270 & 0 & 9.6232 \end{bmatrix}$$

We consider $r(t) = a$, where a can be selected using the final value theorem. The knowledge of a desired state of the reference system is used to determine the vector k_2. From the final value theorem, for the desired trajectory $x_m(t)$ given by Eq. (13), the final value is given by

$$\lim_{t\to\infty} x_m^{\infty}(t) = \lim_{s\to 0} s[sI - (A - BK_1)]^{-1} Bk_2 r(s)$$
$$= -(A - BK_1)^{-1} Bk_2 a = Wk_2 a \tag{34}$$

where $r(s) = \frac{a}{s}$ is the Laplace transform of a, and

$$W = \begin{bmatrix} -0.0081 & 0.0081 & 0.0026 & -0.0026 & -0.0292 & 0.0292 \\ 0.0003 & 0.0003 & 0.0005 & 0.0005 & -0.0001 & -0.0001 \\ 0.0357 & -0.0357 & -0.0517 & 0.0517 & 0.2333 & -0.2333 \end{bmatrix}$$

The rank of W is 3 and since $k_2 \in R^6$, we have an underdetermined system. Therefore, we have to use additional information of the body axis moments of the aircraft model to determine all the components of k_2. For a desired trajectory representing final values of the states:

$$x_{m1}^{\infty}(-0.0752 \text{ deg/s}), \qquad x_{m2}^{\infty}(0 \text{ deg/s})$$
$$x_{m3}^{\infty}(0.4950 \text{ deg/s}) \tag{35}$$

one possible selection of k_2 is to choose the elements of $k_2 = [k_{21}, \ldots, k_{26}]^T$ such that

$$k_{21} = -k_{22}, \qquad k_{23} = k_{24} = 0, \qquad k_{25} = -k_{26}$$

The choice is motivated by the special form that one observes in the matrix W. For a choice of $a = 0.5$ in Eq. (34), arbitrarily selecting two other elements such as $k_{21} = 3.6113$, $k_{25} = 1.5731$, we can determine the other components by a simple solution of linear equations such that k_2 is given by

$$k_2 = [3.6113, \ -3.6113, \ 0, \ 0, \ 1.5731, \ -1.5731]^T$$

The components of k_2 effectively determine the effect of $r(t)$ on our adaptive controller and are chosen such that the coefficient of $k_2 r(t)$ is small enough so that $u_d(t)$ in Eq. (11) has small components and therefore assumption (7) holds. In [12], such an effect has been demonstrated by simulation results. The damping and settling times are also improved. The reference system of Eq. (13) can be built using Eq. (33) and

$$Bk_2 = [-1.7517, \ 0, \ 0.3096]^T$$

In our simulation results, we show that for bounded reference signals which might change at arbitrary instants of time, and those that do not violate the assumption (7), asymptotic state tracking is achieved.

A. Simulation Results

For simulation under assumption (7), we use a reference signal

$$r(t) = \begin{cases} 0.5\sin(t), & 0 \le t \le 50 \\ 0.5\sin(t) + \sin(2t), & t \ge 50 \end{cases} \tag{36}$$

Table 2 Actuator array parameters for simulation

Array: i	Units	1	2	3	4	5	6
θ_{1i}^*	volts-deg	32.8	29.9	26.8	23.8	20.5	17.75
θ_{2i}^*	deg	14.7	13.8	12.8	11.7	10	9.5
$\theta_{1i}(0)$	volts-deg	30	29	26.5	23	20	18
$\theta_{2i}(0)$	deg	15	14	13	12	11	10

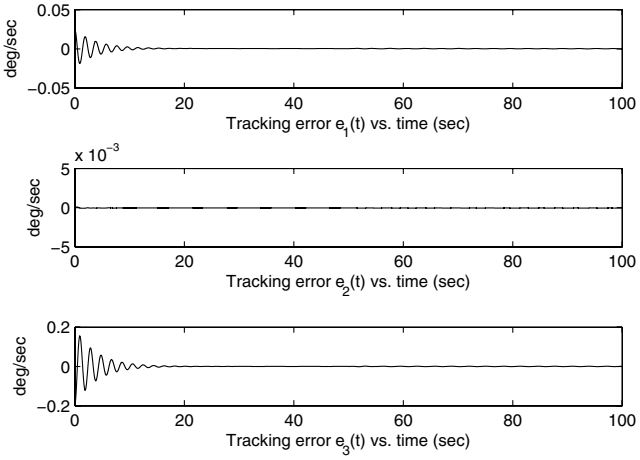

Fig. 9 State tracking errors.

The adaptation gains $\gamma_{1i} = 20$, $\gamma_{2i} = 4$, $i = 1, \ldots, 6$, for our adaptive design, and the nonlinearity parameters are shown in Table 2. The lower bounds of these parameters are assumed as $\theta_{1i}^a = \theta_{2i}^a = 0.1$.

The initial states are assumed as roll rate (0.05 deg/s), pitch rate (0.008 deg/s), and yaw rate (−0.5 deg/s). The initial reference states are assumed as (0.06 deg/s), (0.004 deg/s), and (−0.3 deg/s), respectively.

The results of adaptive inverse array compensation are shown in Figs. 9–13. Specifically, Fig. 9 shows that $e(t)$ asymptotically approach zero. Please note that the presence of transient responses in the tracking errors at 50 s, due to an arbitrary change in reference signal $r(t)$ which instantaneously changes the states $x(t)$ and the reference signals $x_m(t)$, could be expected. The robustness of the adaptation scheme is demonstrated by the fact that the tracking error again approaches zero asymptotically beyond 50 s. Figure 10 shows the controls signals $u_{di}(t)$ generated from Eq. (11). Beyond 50 s, the control signals are governed by the reference signal as given in Eq. (36). The parameter errors converge to fixed constants, which is sufficient for the control objectives of this application. Please note

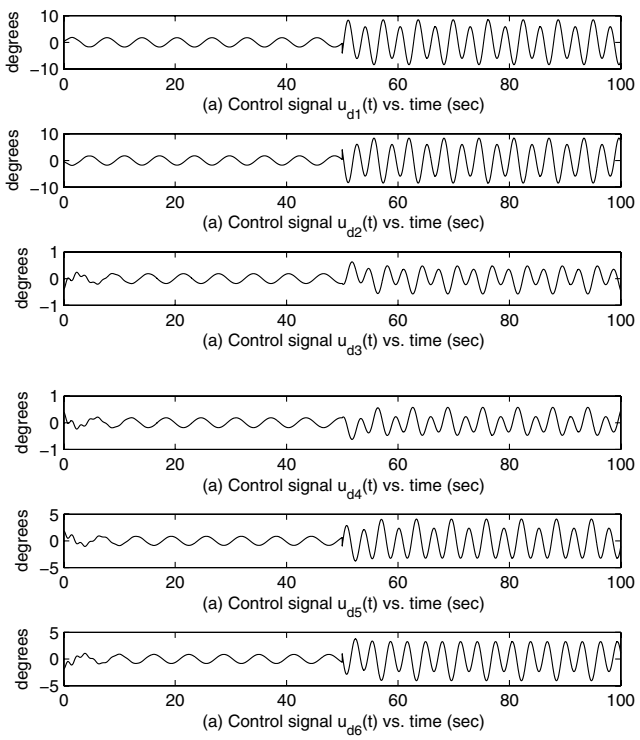

Fig. 10 Control signals $u_{di}(t)$.

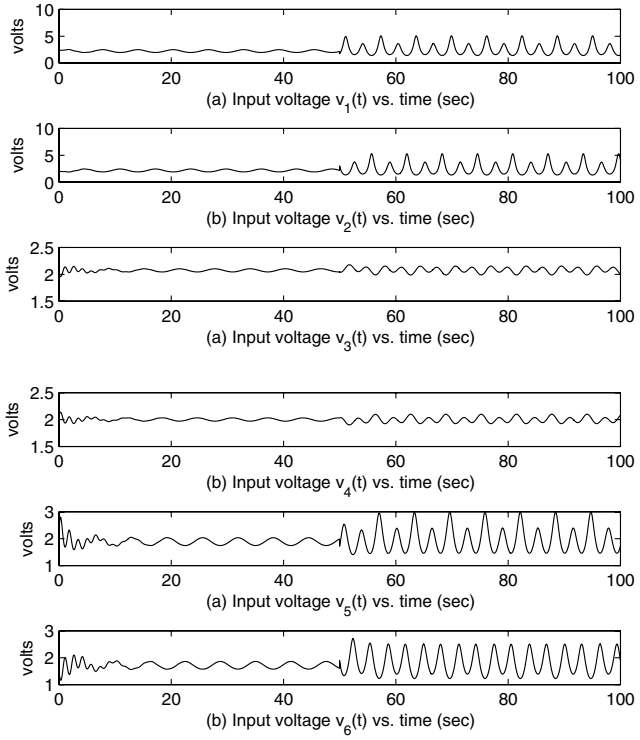

Fig. 11 Input signals $v_i(t)$.

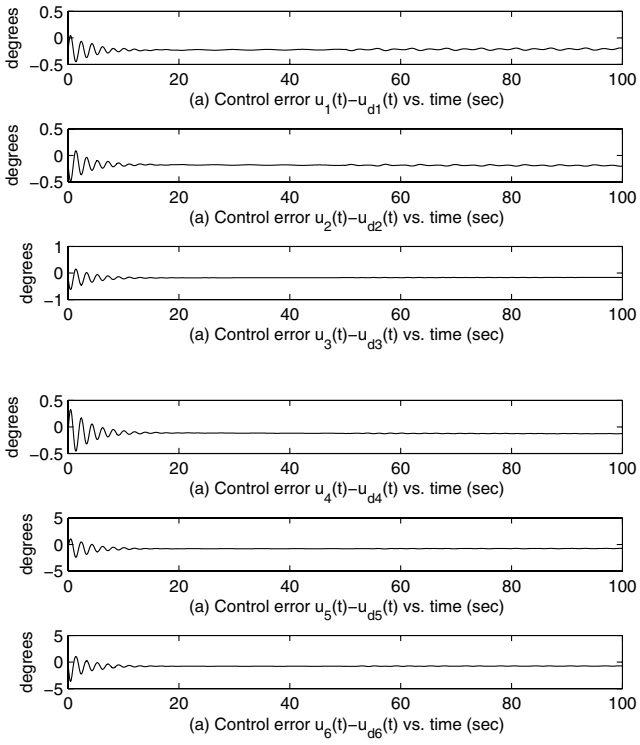

Fig. 12 State tracking errors.

that the approach employed in this paper only guarantees asymptotic state tracking with parameter boundedness.

Figures 11 and 12 show the characteristic signals $v_i(t)$ and $u_i(t) - u_{di}(t)$, respectively. As evident from Eqs. (5) and (9), the signals $v_i(t)$ and $u_i(t) - u_{di}(t)$ are dependent on $r(t)$ given in Eq. (36). This explains the sinusoidal components that are observed in these signals. The effect of the change in $r(t)$ at 50 s is also shown in these plots. Please note that these plots reinforce the fact that the asymptotic tracking of aircraft states has not been achieved at unreasonably high signal amplitudes. The signals $u_i(t) - u_{di}(t)$, $i = 1, \ldots, 6$ do not converge to zero in this particular case. We note that some individual control errors approach some values which are not insignificant. Figure 13 demonstrates that the weighted control error

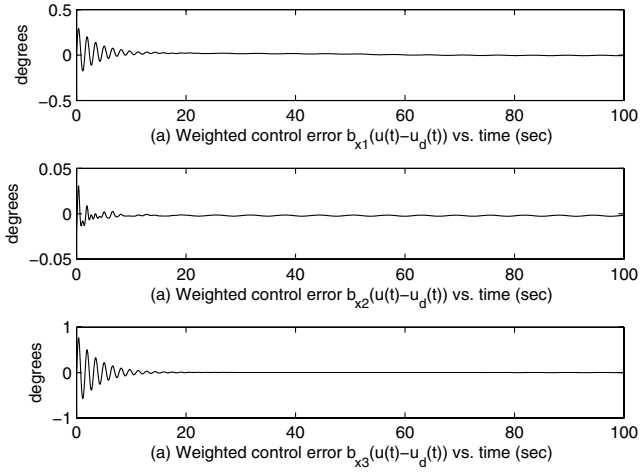

Fig. 13 Weighted control errors.

$$B_x[u(t) - u_d(t)] = \sum_{i=1}^{6} b_i[u_i(t) - u_{di}(t)]$$

where $B_x = [b_{x1}, b_{x2}, b_{x3}]^T$ is the reformulated input matrix obtained from the input matrix $B = [b_1, \ldots, b_6]^T$ and is actually much closer to zero than individual control errors $u_i - u_{di}$, $i = 1, \ldots, 6$ shown in Fig. 12. The oscillatory modes have been effectively canceled by the error system as shown by Fig. 9. These simulation results demonstrate that the asymptotic tracking and stability analysis shown in Theorem VI.1 is achieved.

B. Simulation Results for Disturbance Rejection

We present simulation results for the asymptotic tracking of $x_m(t)$ by $x(t)$ to demonstrate the adaptive control system performance in the presence of the boundary layer imposed disturbances $k_{3i}^* d_i(t)$. We use Table 2, the same initial states and reference states and parameter lower bounds and adaptation gains in the case with no disturbance. Additionally, $d_i(t) = \sin(\omega_i t)$, and $\gamma_{3i} = 1$, $i = 1, \ldots, 6$ are chosen for our adaptive compensation design in the presence of disturbances, and the disturbance parameters are shown in Table 3.

Figure 14 shows that the tracking errors asymptotically go to zero in the presence of an actuation disturbance. The only observed effect of disturbance is that the transience is slightly more pronounced and present for a longer duration. Figure 15 shows that the signals $u_i(t) - u_{di}(t)$, $i = 1, \ldots, 6$ do not all converge to zero as in the no disturbance case. The oscillatory modes have been effectively canceled by the error system. These simulation results corroborate the asymptotic tracking and stability analysis shown in Theorem VI.2.

VIII. Concluding Remarks

This paper presents an adaptive compensation control scheme for virtual aerodynamic wing shaping using synthetic jet actuator arrays. A mathematical model of six synthetic jet actuator arrays, distributed symmetrically about the longitudinal axis of the aircraft, has been

Table 3 Disturbance parameters for simulation

Array: i	Units	1	2	3	4	5	6
k_{3i}^*	deg	0.3	0.3	0.3	0.3	0.3	0.3
ω_i	deg/s	0.2	0.2	0.3	0.3	0.1	0.1
$k_{3i}(0)$	deg	0.21	0.19	0.18	0.23	0.22	0.31

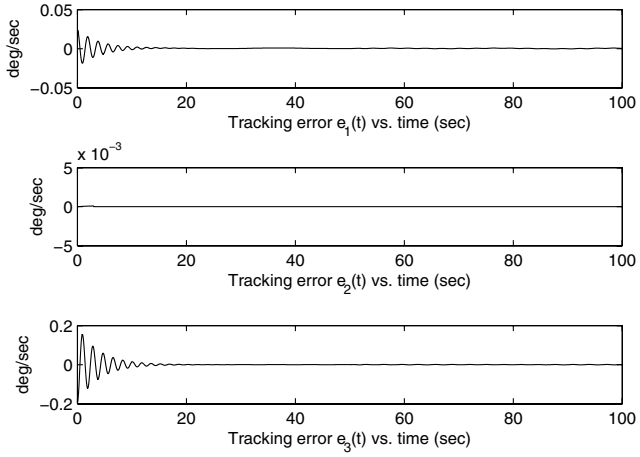

Fig. 14 Tracking errors in presence of disturbance.

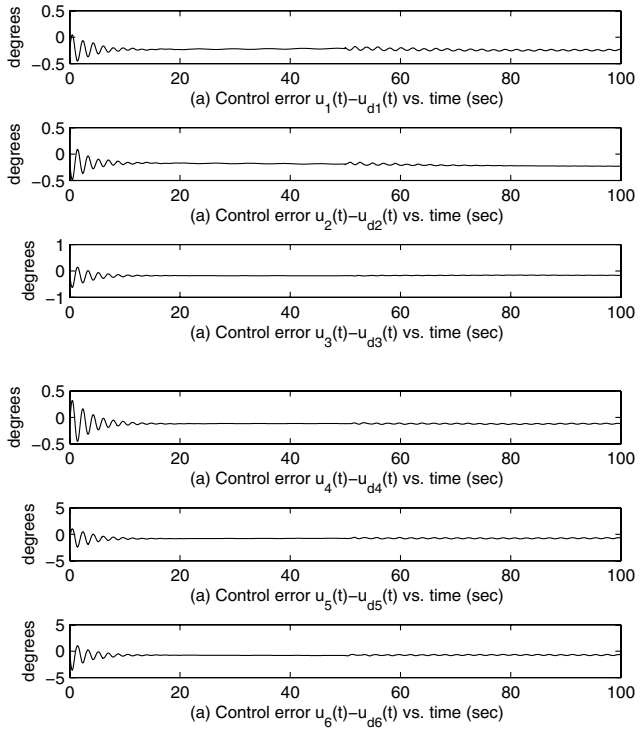

Fig. 15 Control errors $u_i(t) - u_{di}(t)$ in presence of disturbance $k_i^* d_i(t)$.

presented for aircraft flight control. Synthetic jet actuators have inherent nonlinearities of known structure and poorly known parameters. Adaptive inverses have been presented which are capable of adaptively compensating for the actuator parameter uncertainties. State feedback control laws are used for controlling aircraft model dynamics. Parameter projection-based adaptive laws are used to ensure desired closed-loop stability and asymptotic tracking. The adaptation design is robust to gain uncertainties and desired stability and tracking can also be achieved in the presence of bounded disturbances. The new generations of stealth aircrafts designed for reduced radar cross sections lacking vertical surfaces are the most likely platforms for application of synthetic jet actuators. The stability and tracking performance was demonstrated by simulation results on the state information obtained from the linearized model of a nonlinear tailless aircraft model.

IX. Future Challenges

Based on the current results, future work for this research can be formulated. First, a nonlinear feedback control law is to be developed for a nonlinear aircraft dynamic model. Second, an analytical adaptive control framework for tracking of systems with saturation constraints and external disturbances is to be developed. Third, in addition to the jet actuator nonlinearities, there are issues to be addressed with respect to piezoelectric actuator nonlinearities. Fourth, adaptive control algorithms are to be developed for achieving separation control at high angles of attack. It would then be possible to simulate an integrated aircraft control system for virtual surface shaping at low angles of attack for improved performance and efficiency, and flow separation mitigation at high angles of attack for improved safety, and greater control authority. In addition, adaptive compensation of actuator failures also needs to be incorporated so as to obtain optimal performance in the presence of unknown actuator failures.

Acknowledgements

This research was partially supported by the U.S. Air Force under an STTR contract. The authors thank the anonymous reviewers for their insightful comments which have helped us to make significant improvements.

References

[1] Amitay, M., Pitt, D., Kibens, V., Parekh, D. E., and Glezer, A., "Control of Internal Flow Separation Using Synthetic Jet Actuators," AIAA Paper 2000-0903, Jan. 2000.

[2] Smith, D., Amitay, M., Kibens, V., Parekh, D., and Glezer, A., "Modification of the Lifting Body Aerodynamics by Synthetic Jet Actuators," AIAA Paper 98-0209, Jan. 1998.

[3] Amitay, M., Smith, D., Kibens, V., Parekh, D., and Glezer, A., "Aerodynamic Flow Control over an Unconventional Airfoil Using Synthetic Jet Actuators," *AIAA Journal*, Vol. 39, No. 3, 2001, pp. 361–370.

[4] Amitay, M., Horvath, M., Michaux, M., and Glezer, A., "Virtual Aerodynamic Shape Modification at Low Angles of Attack Using Synthetic Jet Actuators," AIAA Paper 2001-2975, Jan. 2001.

[5] Crook, A., and Wood, N. J., "Measurements and Visualizations of Synthetic Jets," AIAA Paper 2001-145, Jan. 2001.

[6] Washburn, A., and Amitay, M., "Active Flow Control on the Stingray UAV: Physical Mechanisms," AIAA Paper 98-0208, Jan. 1998.

[7] Honohan, A., Amitay, M., and Glezer, A., "Aerodynamic Control Using Synthetic Jets," AIAA Paper 2000-2401, 2000.

[8] Chatlynne, E., Rumigny, N., Amitay, M., and Glezer, A., "Virtual Aero-shaping of a Clark-Y Airfoil Using Synthetic Jet Actuators," AIAA Paper 2001-0732, 2001.

[9] Chen, F., and Beeler, G. B., "Virtual Shaping of a Two-Dimensional NACA 0015 Airfoil Using Synthetic Jet Actuator," AIAA Paper 2002-3273, 2002.

[10] Tao, G., *Adaptive Control Design and Analysis*, Wiley, New York, 2003.

[11] Tao, G., and Kokotović, P. V., *Adaptive Control of Systems with Actuator and Sensor Nonlinearities*, Wiley, New York, 1996.

[12] Lockerby, D., "Numerical Simulation of Boundary-Layer Control Using MEMS Actuation," Ph.D. Dissertation, The University of Warwick, March 2001.

[13] Deb, D., Tao, G., Burkholder, J. O., and Smith, D. R., "An Adaptive Inverse Control Scheme for A Synthetic Jet Actuator Model," *Proceedings of the 2005 American Control Conference '05*, 2005.

[14] Deb, D., Tao, G., Burkholder, J. O., and Smith, D. R., "An Adaptive Inverse Control Scheme for Synthetic Jet Actuator Arrays," *Proceedings of the AIAA Infotech@Aerospace Conference '05*, AIAA, Reston, VA, 2005.

[15] Rugh, W. J., *Linear System Theory*, 2nd ed., Prentice–Hall, Englewood Cliffs, NJ, 1996, pp. 146–153.

[16] Lewis. F. L., *Applied Optimal Control and Estimation*, Prentice–Hall, Englewood Cliffs, NJ, 1992, pp. 180–188.

[17] Sastry. S., and Bodson, M., *Adaptive Control: Stability, Convergence, and Robustness*, Prentice–Hall, Englewood Cliffs, NJ, 1989, pp. 161–166.

[18] Le, H., Moin, P., and Kim, J., "Direct Numerical Simulation of Turbulent Flow over a Backward-Facing Step," *AIAA Journal of Fluid Mechanics*, Vol. 330, 1997, pp. 349–374.

[19] Bodson. M., and Douglas, S., "Adaptive Algorithms for the Rejection of Sinusoidal Disturbances with Unknown Frequency," *Automatica*, Vol. 33, No. 12, 1997, pp. 2213–2221.